Int. J. Therm. Sci. (2000) 39, 806–825

S1290-0729(00)00276-3/FLA

A finite volume method to solve the Navier–Stokes equations for incompressible flows on unstructured meshes

Sylvain Boivin [a]*, Florent Cayré [b,c], Jean-Marc Hérard [c]

[a] *Université du Québec à Chicoutimi, 555, Boulevard de l'Université, Chicoutimi, Québec, Canada G7H 2B1*

[b] *Groupe Interdisciplinaire de Recherche en Éléments Finis, Université Laval – Pavillon Adrien Pouliot, Québec, Canada G1K 7P4*

[c] *Département Laboratoire National d'Hydraulique, Groupe Recherches et Études en Thermohydraulique, 6, Quai Watier, BP 49, 78401 Chatou cedex, France*

(Received 11 May 1999, accepted 22 December 1999)

Abstract — A method to solve the Navier–Stokes equations for incompressible viscous flows and the convection and diffusion of a scalar is proposed in the present paper. This method is based upon a fractional time step scheme and the finite volume method on unstructured meshes. A recently proposed diffusion scheme with interesting theoretical and numerical properties is tested and integrated into the Navier–Stokes solver. Predictions of Poiseuille flows, backward-facing step flows and lid-driven cavity flows are then performed to validate the method. We finally demonstrate the versatility of the method by predicting buoyancy force driven flows of a Boussinesq fluid (natural convection of air in a square cavity with Rayleigh numbers of 10^3 and 10^6). © 2000 Éditions scientifiques et médicales Elsevier SAS

Navier–Stokes / finite volume method / unstructured mesh / fractional time step / diffusion scheme / lid-driven cavity flow / Boussinesq fluid / natural convection / buoyancy force

Résumé — Une méthode des volumes finis pour la résolution des équations de Navier–Stokes pour des écoulements incompressibles à maillages non structurés. Cet article propose une méthode de résolution des équations de Navier–Stokes pour les écoulements visqueux incompressibles et la convection et diffusion d'un scalaire. Celle-ci est basée sur un schéma à pas de temps fractionnaire et la méthode des volumes finis sur maillages non structurés. Un schéma pour la diffusion, proposé récemment, dont les propriétés théoriques et numériques sont intéressantes, est testé puis intégré dans un solveur des équations de Navier–Stokes. Des simulations d'écoulement de Poiseuille, de marche descendante et de cavité carrée entraînée, ont permis de valider la méthode. Enfin, la polyvalence de la méthode est illustrée par des simulations d'écoulement d'un fluide de Boussinesq soumis à la poussée d'Archimède (convection naturelle d'air dans une cavité carrée, pour des nombres de Rayleigh de 10^3 et 10^6). © 2000 Éditions scientifiques et médicales Elsevier SAS

Navier–Stokes / méthode des volumes finis / maillage non structuré / pas de temps fractionnaire / schéma pour la diffusion / cavité carrée entraînée / fluide de Boussinesq / convection naturelle / poussée d'Archimède

1. INTRODUCTION. MATHEMATICAL MODEL

Although many stable, convergent and globally conservative numerical schemes are already available to solve the Stokes equations, most industrial problems are governed by the more general Navier–Stokes equations. Moreover, they are often coupled with an additional equation, in order to model the convection and diffusion of a scalar quantity such as temperature, pollutant concentration or turbulent kinetic energy. Among the existing methods dedicated to these problems, just a few fulfill the following physical principles:

- local conservation of the mass and the scalar quantities,
- numerical preservation of the *maximum principle* for the scalar quantities.

Some numerical schemes using the finite volume method on structured meshes can deal with these requirements. However, only a few results are available on unstructured meshes (see [1–3] for hyperbolic systems,

* Correspondence and reprints.
sboivin@uqac.uquebec.ca

[1, 2, 4–8] for elliptic systems, and [1, 2, 14] for parabolic systems).

The scheme presented hereafter fulfills the two previous requirements on unstructured triangular meshes. It is based on a fractional time-step method initially proposed in [9], but integrates a recent interesting diffusion scheme proposed in [2], which was first separately tested.

The method does not require to assemble any matrix, and the number of arithmetical operations to perform is small. Following is a short recall of the mathematical model.

The flow of an incompressible fluid in a domain $\Omega \times [0, T]$ is governed by the Navier–Stokes equations:

$$\nabla \cdot \boldsymbol{u} = 0 \tag{1}$$

$$\frac{\partial \boldsymbol{u}}{\partial t} + \nabla \cdot (\boldsymbol{u} \otimes \boldsymbol{u}) + \nabla p - \nabla \cdot (\nu \nabla \boldsymbol{u}) = \boldsymbol{f} \tag{2}$$

where

- p stands for P/ρ_0, with ρ_0 being the density and P being the pressure of the incompressible fluid,
- ν is the constant kinematic viscosity of the fluid: $\nu = \mu_0/\rho_0$, with μ_0 being the constant dynamic viscosity.

A model of the convection and diffusion of a passive scalar quantity in the flow is then

$$\frac{\partial C}{\partial t} + \nabla \cdot (C\boldsymbol{u}) - \nabla \cdot (\kappa \nabla C) = s \tag{3}$$

with κ being the constant diffusivity of the scalar quantity C.

Note that these equations must come with suitable boundary conditions, so that the problem has a unique solution. The field of industrial applications of this model extends to the prediction of pollutant transport and heat transfer, by adjusting the source terms to the corresponding problem.

The present paper is organized as follows. First of all, the time discretization of the Navier–Stokes equations coupled with some governing equation for a pollutant is recalled. Afterwards, spatial schemes used to account for convective terms, viscous terms, mean pressure gradient effects and source terms associated with momentum or scalar equations are recalled, *focusing on triangular meshes*. Theoretical rates of convergence obtained recently by other authors are recalled in this section. Suitable ways to implement boundary conditions are also discussed. The whole allows to introduce some way to compute some unsteady convection–diffusion equation involving source terms. Hence one may propose a fractional step method which first provides some approximation of the velocity field, and then updates both the velocity and pressure fields in an implicit way, so that the divergence-free constraint for the velocity field is ensured. The projection step is based on the use of a special property of triangles (or its counterpart, say tetrahedra in the three-dimensional case) to reconstruct the velocity field within each cell in such a way that normal components of velocities are continuous on each cell interface. The projection step requires solving an elliptic equation and thus investigating the real rate of convergence of a recently analyzed diffusion scheme nicknamed VF4, which in fact is the straightforward counterpart of the well-known VF5 scheme which is widely used when using rectangle Finite Volume methods. This eventually enables presenting the whole algorithm proposed to solve incompressible Navier–Stokes equations on unstructured triangular meshes which do not necessarily agree with the Delaunay condition. Above mentioned requirements are shown to be fulfilled on any kind of mesh, provided that one uses some adequate reconstruction method when some IOB commute in the mesh, and obviously some suitable way to compute local source terms.

Intensive validation of the diffusive scheme is then provided. Convergence rates will be shown to be one order greater than the theoretical one, considering regular enough analytical solutions of the Poisson equation, with different boundary conditions. The scheme is also proved to converge (with reduced convergence rate) when computing Green functions with some singular point inside the computational domain. This study clearly shows that the discrete unknowns represent optimal approximations of the unknown function at the IOB, and thus also at the cell center—but in that case the measured convergence rate is reduced by one. This of course has motivated the need to reconstruct better (namely, second-order) approximations of the unknowns at the cell center of control volumes, using some linear fitting which fortunately is proved *in practice* to permit retrieving the *discrete maximum principle* on triangular meshes which do not satisfy Delaunay condition.

Following numerical results aim at showing the capabilities of the present scheme to solve full Navier–Stokes equations. These include Poiseuille flow, the computation of the lid-driven cavity flow and the backward facing step. Eventually, an example of the versatility of the scheme is illustrated in Section 5.5 by the computation of natural convection of air in a square cavity. Convergence history towards steady states is illustrated.

Appendix A provides some way to get accurate enough approximations of unknowns on cell centers, on the basis of approximations at the intersection of orthogonal bisectors of triangle interfaces. Particular emphasis is given in

Appendix B on the numerical treatment of source terms pertaining to scalar equations when some *maximum principle* is involved. Any kind of source term may thus be implemented provided that its form is such that the maximum principle is ensured at the *continuous* level.

2. TIME DISCRETIZATION

The time discretization used here is based upon a variation of the projection scheme originally proposed by Chorin (see [10]):

- Prediction:

$$\frac{\boldsymbol{u}^{n+1/2}-\boldsymbol{u}^{n}}{\delta t}+\nabla\left(\boldsymbol{u}^{n+1/2}\otimes\boldsymbol{u}^{n}\right) - \nabla\cdot\left(\nu\nabla\boldsymbol{u}^{n+1/2}\right)+\nabla p^{n}=\boldsymbol{f}^{n} \tag{4}$$

- Projection:

$$\frac{\boldsymbol{u}^{n+1}-\boldsymbol{u}^{n+1/2}}{\delta t}+\nabla\left(p^{n+1}-p^{n}\right)=0 \tag{5}$$

$$\nabla\cdot\boldsymbol{u}^{n+1}=0 \tag{6}$$

- Convection–diffusion of the passive scalar C:

$$\frac{C^{n+1}-C^{n}}{\delta t}+\nabla\cdot\left(\boldsymbol{u}^{n+1}C^{n+1}\right)-\nabla\cdot\left(\kappa\nabla C^{n+1}\right)=s^{n} \tag{7}$$

where s^n is supposed to be regular enough ($s^n \in L^2(\Omega)$), Ω being the computational domain). Note that the equations (5) and (6) are used below under the following form:

$$\nabla\cdot\boldsymbol{u}^{n+1/2}-\delta t\,\Delta\left(p^{n+1}-p^{n}\right)=0 \tag{8}$$

$$\boldsymbol{u}^{n+1}=\boldsymbol{u}^{n+1/2}-\delta t\nabla\left(p^{n+1}-p^{n}\right) \tag{9}$$

3. SPACE DISCRETIZATION

The convection and diffusion schemes are presented thereafter. The convection scheme is simple and robust. Its accuracy could easily be improved using a reconstruction method such as MUSCL.

We insist here particularly on the diffusion scheme, which is an essential part of the global solver. It was proposed in [2], which is not published at the time we write this paper. A numerical study was performed in the report [11], where the scheme was proved to be accurate and preserve the maximum principle, even on poor quality meshes, which is crucial for industrial applications. The main results of this study are presented in Section 5.1.

Properties concerning the combination of both following schemes into a convection–diffusion equation are pointed out at the end of this section, and Appendix B is dedicated to the preservation of the maximum principle with source terms.

3.1. The convection scheme

The convection scheme used in the following is an upwind scheme. The term to be approximated is

$$\int \boldsymbol{u}\cdot\nabla\phi\,\mathrm{d}\Omega=\int\nabla\cdot(\boldsymbol{u}\phi)\,\mathrm{d}\Omega \tag{10}$$

with ϕ being the convected variable and $\boldsymbol{u}$ the velocity, in agreement with $\nabla\cdot\boldsymbol{u}=0$.

A discretization of (10) can be obtained by integration on each triangle T, followed by the application of the Stokes theorem:

$$\int_T \nabla\cdot(\boldsymbol{u}\phi)\,\mathrm{d}\Omega=\oint_{\partial T}\phi\boldsymbol{u}\cdot\boldsymbol{n}\,\mathrm{d}\Gamma$$

with $\boldsymbol{n}$ being the outward normal unit vector and ∂T the boundary of the triangle.

3.1.1. Definition inside the domain

Assuming $\phi_{\mathrm{h}}(T_i)$ and $\phi_{\mathrm{h}}(T_j)$ denote the approximations[1] of the variable ϕ in the adjacent triangles T_i and T_j, the convective term on their common edge σ_{ij} is given by

$$\int_{\sigma_{ij}}\phi\boldsymbol{u}\cdot\boldsymbol{n}\,\mathrm{d}\Gamma \simeq l_{\sigma_{ij}}(\boldsymbol{u}_{\mathrm{h}}\cdot\boldsymbol{n})_{\sigma_{ij}}\left[\left(\alpha_{ij}\phi_{\mathrm{h}}(T_i)+(1-\alpha_{ij})\phi_{\mathrm{h}}(T_j)\right)\right]$$

where $l_{\sigma_{ij}}$ denotes the length of the edge σ_{ij}, $\boldsymbol{n}$ denotes the normal unit vector directed from T_i to T_j, and

$$\alpha_{ij}=\begin{cases}1 & \text{if } (\boldsymbol{u}_{\mathrm{h}}\cdot\boldsymbol{n})_{\sigma_{ij}}>0\\ 0 & \text{otherwise}\end{cases}$$

[1] Note that $\phi(T_i)$ and $\phi(T_j)$ are not necessarily the chosen discrete unknowns for the variable ϕ, but are good approximations of the variable *inside* the triangles T_i and T_j. As will be seen later, the discrete unknown associated to a triangle can indeed be the best approximation of ϕ *outside* this triangle.

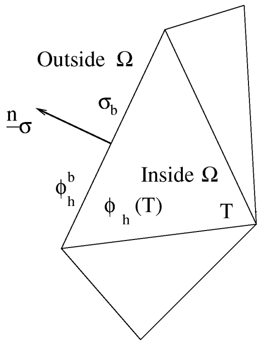

σ_{b} an edge on the boundary of the domain Ω

$\boldsymbol{n}_\sigma$ the outward normal unit vector of the edge σ_{b}

$\phi_{\mathrm{h}}^{\mathrm{b}}$ the value of the variable ϕ on the edge σ_{b}

$\phi_{\mathrm{h}}(T)$ the value of the variable ϕ in the triangle T

Figure 1. Boundary conditions for the convection operator.

3.1.2. Boundary conditions

For a given boundary edge σ_{b} (see *figure 1*):

- if the fluid is incoming (i.e. $(\boldsymbol{u}\cdot\boldsymbol{n})_{\sigma_{\mathrm{b}}} < 0$):

$$\int_{\sigma_{\mathrm{b}}} \phi \boldsymbol{u}\cdot\boldsymbol{n}\,\mathrm{d}\Gamma \simeq l_{\sigma_{\mathrm{b}}}(\boldsymbol{u}\cdot\boldsymbol{n})_{\sigma_{\mathrm{b}}}\phi_{\mathrm{h}}^{\mathrm{b}}$$

where $(\boldsymbol{u}\cdot\boldsymbol{n})_{\sigma_{\mathrm{b}}}$ and $\phi_{\mathrm{h}}^{\mathrm{b}}$ stand for the prescribed values of ϕ and $\boldsymbol{u}\cdot\boldsymbol{n}$ on the inlet boundary,

- if the fluid is outcoming (i.e. $(\boldsymbol{u}\cdot\boldsymbol{n})_{\sigma_{\mathrm{b}}} > 0$):

$$\int_{\sigma_{\mathrm{b}}} \phi \boldsymbol{u}\cdot\boldsymbol{n}\,\mathrm{d}\Gamma \simeq l_{\sigma_{\mathrm{b}}}(\boldsymbol{u}\cdot\boldsymbol{n})_{\sigma_{\mathrm{b}}}\phi_{\mathrm{h}}(T)$$

where T denotes the triangle including the boundary edge σ_{b}.

3.1.3. Theoretical results

The convergence of this upwind scheme is analyzed [3] with an explicit Euler time discretization. It is proved that under a CFL condition, the scheme converges and the rate of convergence is $1/2$.

3.2. The diffusion scheme

Following is a short summary of the properties established in the still unpublished book [2], and that interest us directly.

Consider the elliptic problem:

$$\begin{cases} -\Delta u = f \\ \text{boundary conditions} \end{cases} \tag{11}$$

where the set of boundary conditions is assumed to be such that the problem is well posed.

Let $(T_i)_{i\in\{1,2,\ldots,N\}}$ be a triangulation of the domain Ω. For each triangle T_i, let S_i be its surface, E_i the set of its edges, and u_i its associated discrete unknown.

Integrating (11) on T_i and using the Stokes theorem yields

$$-\sum_{\sigma\in E_i} F_\sigma^{\mathrm{D}}(u_{\mathrm{h}}) = S_i f_i \tag{12}$$

where f_i stands for $(1/S_i)\int_{T_i} f(x)\,\mathrm{d}x$, $F_\sigma^{\mathrm{D}}(u_{\mathrm{h}})$ is an approximation of $\int_\sigma \nabla u\cdot\boldsymbol{n}_{\sigma,T_i}\,\mathrm{d}s$, where $\boldsymbol{n}_{\sigma,T_i}$ is the outward normal unit vector of the edge σ of T_i.

The expression of $F_\sigma^{\mathrm{D}}(u_{\mathrm{h}})$ must be determined both for edges inside the domain and on the boundary.

3.2.1. Definition inside the domain

For each triangle T_i, let $\boldsymbol{x}_i$ be the intersection of the orthogonal bisectors (IOB) of the edges (see *figure 2*). This point is outside T_i in the case of a triangle that has one angle strictly larger than $\pi/2$. It is on an edge if T_i is a right-angled triangle.

We assume here that the edge σ_{ij} is common to the two triangles T_i and T_j and that $\boldsymbol{x}_i \neq \boldsymbol{x}_j$. The case of equality will be discussed in Section 5.1.

The expression of the associated numerical flux $F_{\sigma_{ij}}^{\mathrm{D}}(u_{\mathrm{h}})$ is

$$F_{\sigma_{ij}}^{\mathrm{D}}(u_{\mathrm{h}}) = l_{ij}\,\frac{u_j - u_i}{(\boldsymbol{x}_j - \boldsymbol{x}_i)\cdot\boldsymbol{n}_{ij}} \tag{13}$$

where $\boldsymbol{n}_{ij} = \boldsymbol{n}_{\sigma_{ij},T_i}$ is the outward normal unit vector of the edge σ_{ij} of T_i.

The following coefficient called *transmittivity* is introduced in [2] for each internal edge σ_{ij} under the assumption $\boldsymbol{x}_i \neq \boldsymbol{x}_j$:

$$\tau_{\sigma_{ij}} = \frac{l_{ij}}{(\boldsymbol{x}_j - \boldsymbol{x}_i)\cdot\boldsymbol{n}_{ij}}$$

With this definition, (13) can be reformulated as

$$F_{\sigma_{ij}}^{\mathrm{D}}(u_{\mathrm{h}}) = \tau_{\sigma_{ij}}(u_j - u_i)$$

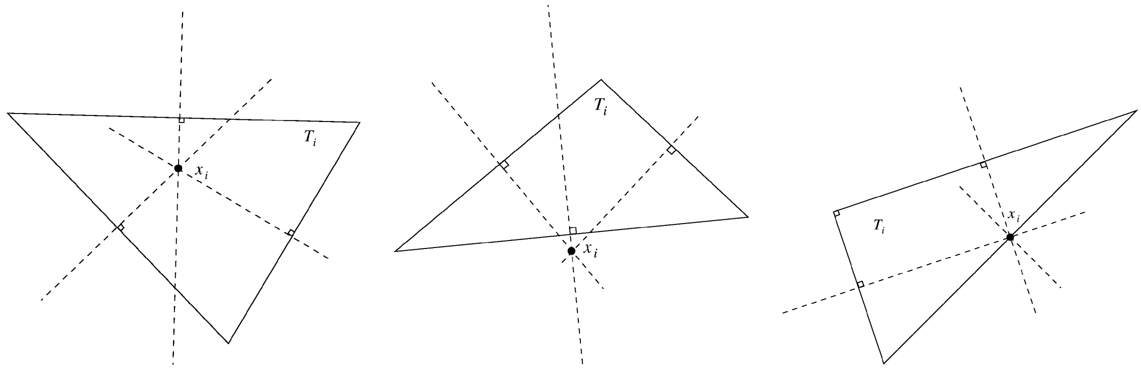

(1) Every angle is less than $\pi/2$ (2) One angle is larger than $\pi/2$ (3) One angle is equal to $\pi/2$

Figure 2. Intersection of the orthogonal bisectors of the edges of a triangle.

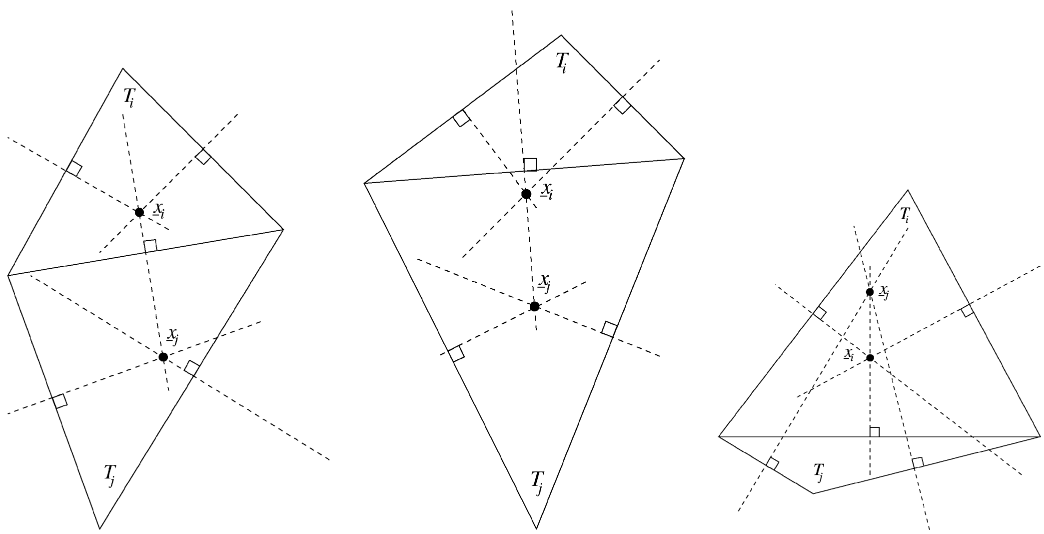

Category M_1 Category M_2 Category M_3

Figure 3. Different categories of meshes.

3.2.2. Boundary conditions

If the boundary condition applied to the edge σ is a Neumann boundary condition, the numerical flux F_σ is equal to the exact flux.

Where a Dirichlet boundary condition applies, the value u_σ is given at the middle point x_σ of the boundary edge σ. Let T_i be the triangle of the mesh including σ, and $\boldsymbol{x}_i$ its IOB. Assuming that $\boldsymbol{x}_\sigma \neq \boldsymbol{x}_i$, the numerical flux is then

$$F_\sigma^{\mathrm{D}}(u_{\mathrm{h}}) = l_\sigma \, \frac{u_\sigma - u_i}{(\boldsymbol{x}_\sigma - \boldsymbol{x}_i) \cdot \boldsymbol{n}_{\sigma,T_i}} \tag{14}$$

The transmittivity can be defined for the boundary edge σ as well (under the assumption $\boldsymbol{x}_\sigma \neq \boldsymbol{x}_i$):

$$\tau_\sigma = \frac{l_\sigma}{(\boldsymbol{x}_\sigma - \boldsymbol{x}_i) \cdot \boldsymbol{n}_{\sigma,T_i}}$$

and then

$$F_\sigma^{\mathrm{D}}(u_{\mathrm{h}}) = \tau_\sigma (u_\sigma - u_i)$$

3.2.3. Theoretical results

The properties shown in [2] depend of the quality of the triangulation $(T_i)_{\{i \in 1,2,\ldots,N\}}$. Three different categories of meshes are introduced in the following (see *figure 3*):

• The category "M_1" contains the so-called "admissible meshes" introduced in [2], which are triangulations such that

$$x_i \in T_i, \qquad \forall i \in \{1, 2, \ldots, N\} \tag{15}$$

$$x_i \neq x_j, \qquad \forall (i, j) \in \{1, 2, \ldots, N\}^2 / T_i \cap T_j \neq \emptyset \tag{16}$$

$$x_i \neq x_\sigma, \qquad \forall i \in \{1, 2, \ldots, N\} / T_i \cap \partial\Omega = \sigma \tag{17}$$

Conditions (16) and (17) are necessary for the transmittivity τ_σ to exist for each edge σ of the mesh. Equation (16) ensures that two adjacent triangles have distinct IOB (they might be both on the common edge of the triangle). Equation (15) implies that τ_σ is positive.

• The category "M_2" is the subset of the non-admissible meshes which satisfy the conditions (16), (17) and

$$\tau_\sigma > 0, \quad \forall i \in \{1, 2, \ldots, N\},\ \forall \sigma \in E_i \tag{18}$$

The only difference with the previous category of meshes is that the IOB of a triangle can be outside of this triangle.

• The meshes that are not included in the two previous categories form the category "M_3". A particular case of this category is a mesh for which the transmittivity is not defined for all the edges. This case will be discussed in Section 5.1. The usual case corresponds with permutation of two IOB connected with two adjacent triangles.

The following properties were shown in [2]:

1. *Convergence*. If the mesh belongs to the categories M_1, the previous scheme converges to the unique solution of the problem (11).

2. *Error estimate*. If the mesh τ belongs to the category M_1 and the unique solution u of the problem (11) is regular enough ($u \in C^2(\Omega)$), we have the following error estimate:

$$\|e_\tau\|_{L^2(\Omega)} \leq Ch \tag{19}$$

where
• $e_\tau(x) = u(x_i) - u_i$, $\forall x \in T_i$, $\forall i \in \{1, 2, \ldots, N\}$,
• C is a positive real number,
• h is the mesh size (for example, the length of the longest edge).

3. *Maximum principle*. If the mesh belongs to one of the categories M_1 and M_2, the discrete maximum principle is preserved (cf. [2] for details).

Numerical convergence of the diffusion scheme is studied in Section 5.1. The very interesting properties demonstrated therein are essential for the quality of the global solver: the scheme is not only used within the prediction step (diffusion of the velocity components), but its accuracy is also crucial in the projection step, as will be emphasized in Section 4.1.3.

For a convection and diffusion equation such as (3), the theoretical rate of convergence obtained with the schemes of the Sections 3.1 and 3.2 is $1/2$, due to the rate of convergence of the convection scheme (see Section 3.1.3 and [1, 2, 12]). In Appendix B it is proved that the discrete maximum principle is preserved when solving a convection–diffusion equation with source terms, under the assumptions that the mesh belongs to category M_1 or M_2, and the source terms preserve the continuous maximum principle and are properly discretized.

4. GLOBAL SCHEME OF THE NAVIER–STOKES SOLVER

Some operators are defined below, which will be used in the presentation of the complete Navier–Stokes scheme.

4.1. Definition of the operators

4.1.1. Convection and diffusion operator CD_s

In this section, we discretize the following equation on the domain Ω:

$$\frac{w^* - w^n}{\delta t} + \nabla \cdot \left(\boldsymbol{u}^n w^*\right) - \nabla \cdot \left(\nu \nabla w^*\right) = s^n \tag{20}$$

where

• s^n is a source term (see Appendix B for details on its discretization),

• the variable w can be either u_x, u_y (the two coordinates of the speed $\boldsymbol{u}$) or C (a passive scalar): see equations (4) and (7),

• $\boldsymbol{u}^n$ is such that $\nabla \cdot \boldsymbol{u}^n = 0$.

The discrete form is obtained by integrating (20) on each triangle T_i:

$$\int_{T_i} \left(\frac{w_\mathrm{h}^* - w_\mathrm{h}^n}{\delta t} + \nabla_\mathrm{h} \cdot \left(\boldsymbol{u}_\mathrm{h}^n w_\mathrm{h}^*\right) - \nabla \cdot \left(\nu \nabla_\mathrm{h} w_\mathrm{h}^*\right)\right) \mathrm{d}\Omega = \int_{T_i} s_\mathrm{h}^n \, \mathrm{d}\Omega$$

where $\boldsymbol{u}_\mathrm{h}^n$ is supposed to fulfill the following conditions:

- for each edge σ common to the triangles T_i and T_j (continuity of the normal value on each edge)

$$\boldsymbol{u}_{\mathrm{h}}^{n} \cdot \boldsymbol{n}_{\sigma,T_i} = -\boldsymbol{u}_{\mathrm{h}}^{n} \cdot \boldsymbol{n}_{\sigma,T_j} = \left(\boldsymbol{u}_{\mathrm{h}}^{n} \cdot \boldsymbol{n}\right)_{\sigma} \tag{21}$$

- $\boldsymbol{u}_{\mathrm{h}}^{n}$ is a divergence-free velocity field in the following sense:

$$\forall i \in \{1, 2, \ldots, N\}, \quad \sum_{\sigma \in E_i} l_\sigma \left(\boldsymbol{u}_{\mathrm{h}}^{n} \cdot \boldsymbol{n}\right)_{\sigma} = 0 \tag{22}$$

The convective and diffusive terms are computed as presented in Sections 3.1 and 3.2, respectively. The numerical properties of the diffusion scheme (see Section 5.1), and the discrete form of the source terms (see Appendix B), are of particular importance in the case where a maximum principle has to be preserved.

Given the results of Section 3.2 and Appendix A, the discrete unknowns are chosen to be approximations of their respective variable at the IOB of the triangles. However, as noticed in Section 3.1, an approximation of the convected variable w *inside* the triangle should be used for the convective term. Therefore, the value chosen for the convection is the approximation of w at the center of gravity of the triangle, computed as in Appendix A.2.4. This value, denoted $G_i(w_{\mathrm{h}})$, can also be used within the term of the time derivation in order to increase accuracy, but concerning the convection scheme, this value is of particular importance as the stability of the scheme may depend on it (see Appendix A).

The discrete form of the equation (20) for a triangle T_i is

$$S_i \frac{G_i(w_{\mathrm{h}}^*) - G_i(w_{\mathrm{h}}^n)}{\delta t} + \sum_{\sigma \in E_i} l_\sigma \boldsymbol{u}_{\mathrm{h}}^{n} \cdot \boldsymbol{n}_{\sigma,T_i} G_\sigma\left(w_{\mathrm{h}}^*\right) - \nu \sum_{\sigma \in E_i} F_\sigma^{\mathrm{D}}\left(w_{\mathrm{h}}^*\right) = S_i s_i^n \tag{23}$$

where

- S_i is the surface of the triangle T_i,
- $G_\sigma(w_{\mathrm{h}}^*)$ depends on the type of edge:
  - ∗ if σ is an internal edge, common to T_i and T_j, then

$$G_\sigma\left(w_{\mathrm{h}}^*\right) = \alpha_{ij} G_i\left(w_{\mathrm{h}}^*\right) + (1-\alpha_{ij}) G_j\left(w_{\mathrm{h}}^*\right) \quad \text{where} \quad \alpha_{ij} = \begin{cases} 1 & \text{if } (\boldsymbol{u}_{\mathrm{h}} \cdot \boldsymbol{n})_{\sigma_{ij}} > 0 \\ 0 & \text{otherwise} \end{cases}$$

  - ∗ if σ is a boundary edge where the fluid is incoming (i.e. $\boldsymbol{u}_{\mathrm{h}}^{n} \cdot \boldsymbol{n}_{\sigma,T_i} < 0$), then

$$G_\sigma\left(w_{\mathrm{h}}^*\right) = w_{\mathrm{h}}^{\mathrm{b}}$$

  - ∗ if σ is a boundary edge where the fluid is outcoming (i.e. $\boldsymbol{u}_{\mathrm{h}}^{n} \cdot \boldsymbol{n}_{\sigma,T_i} > 0$), then

$$G_\sigma\left(w_{\mathrm{h}}^*\right) = w_i^*$$

- $F_\sigma^{\mathrm{D}}(w_{\mathrm{h}}^*)$ is the diffusion flux computed as in Section 3.2.

The system (23) is linear but not symmetric. The associated matrix is a diagonal dominant M-matrix. The system can be solved using an iterative method such as Newton–GMRES. This method uses only residuals of the system, so that the matrix does not need to be built. Moreover, this method handles nonlinear source terms, which is often useful in industrial applications.

The solution w_{h}^* of the system will be denoted $CD_s(w_{\mathrm{h}}^n)$. The convection and diffusion of the approximate velocity $\boldsymbol{u}_{\mathrm{h}}^{n}$ itself can be considered as the convection and diffusion of its two coordinates independently. Therefore, we can also use the notation $\boldsymbol{u}_{\mathrm{h}}^{*} = CD_s(\boldsymbol{u}_{\mathrm{h}}^{n})$. Note that $\boldsymbol{u}_{\mathrm{h}}^{n}$ fulfills conditions (21) and (22), but $\boldsymbol{u}_{\mathrm{h}}^{*}$ does not. Therefore, the two following operators correct the velocity field so that it fulfills first (21), then (21) and (22).

4.1.2. Extension operator E

This operator is applied on an approximation of the velocity denoted $\boldsymbol{u}_{\mathrm{h}}^{*}$, which normal value on the edge of the triangles is not continuous. Its result, denoted $\boldsymbol{u}_{\mathrm{h}}^{**} = E(\boldsymbol{u}_{\mathrm{h}}^{*})$, is defined by a unique value of $\boldsymbol{u}_{\mathrm{h}}^{**} \cdot \boldsymbol{n}_\sigma$ on each given edge σ of the mesh, as follows.

- If σ is an internal edge, common to the triangles T_i and T_j, then

$$\boldsymbol{u}_{\mathrm{h}}^{**} \cdot \boldsymbol{n}_{\sigma,T_i} = t_{ij} \times \left(u_i^* \cdot \boldsymbol{n}_{\sigma,T_i}\right) + (1 - t_{ij}) \times \left(\boldsymbol{u}_j^* \cdot \boldsymbol{n}_{\sigma,T_i}\right)$$

The coefficient t_{ij} was introduced in Appendix A.2.1. The expression above is an interpolation on the edge of the projections on $\boldsymbol{n}_{\sigma,T_i}$ of the speed in the triangles T_i and T_j.

- If σ is a boundary edge where the value g_σ of the normal speed is given, then

$$\boldsymbol{u}_{\mathrm{h}}^{**} \cdot \boldsymbol{n}_{\sigma,T_i} = g_\sigma$$

This case corresponds to a wall, or a boundary where the fluid is incoming.

- If σ is a boundary edge where the value of the normal speed is not given, then

$$\boldsymbol{u}_{\mathrm{h}}^{**} \cdot \boldsymbol{n}_{\sigma,T_i} = \boldsymbol{u}_i^* \cdot \boldsymbol{n}_{\sigma,T_i}$$

This case corresponds to a boundary where the fluid is outcoming.

4.1.3. Projection operator P

This operator applies to both the pressure and the velocity:

$$P : \left(p_\mathrm{h}^n, \boldsymbol{u}_\mathrm{h}^{**}\right) \longmapsto \left(p_\mathrm{h}^{n+1}, \boldsymbol{u}_\mathrm{h}^{n+1}\right)$$

This operation is carried out in two steps, corresponding to the discretization of the equations (8) and (9). Denoting $\delta p = p^{n+1} - p^n$:

$$\nabla \cdot \boldsymbol{u}^{**} - \delta t \, \Delta(\delta p) = 0 \tag{24}$$

$$\boldsymbol{u}^{n+1} = \boldsymbol{u}^{**} - \delta t \nabla(\delta p) \tag{25}$$

The equation (24) is a diffusion problem for the pressure increment δp with a source term. It is solved as in Section 3.2. The second-order accuracy obtained in the numerical tests of the diffusion scheme (see Section 5.1) is particularly interesting, as it makes it possible to get the first-order accuracy for the velocity field correction in this step.

Integrating on a triangle T_i, which set of edges is E_i, yields

$$-\sum_{\sigma \in E_i} F_\sigma^\mathrm{D}(\delta p) = -\frac{1}{\delta t} \sum_{\sigma \in E_i} l_\sigma \boldsymbol{u}_\mathrm{h}^{**} \cdot \boldsymbol{n}_{\sigma, T_i}$$

which has the same form as equation (12), and can therefore be solved the same way. Since the matrix of the corresponding system is symmetric and positive, an iterative conjugate gradient algorithm can be used, so that we do not need to build the matrix.

The equation (25) is then discretized as

$$\left(\boldsymbol{u}^{n+1} \cdot \boldsymbol{n}\right)_\sigma = \left(\boldsymbol{u}^{**} \cdot \boldsymbol{n}\right)_\sigma - \frac{\delta t}{l_\sigma} F_\sigma^\mathrm{D}(\delta p)$$

for each edge σ of the mesh. Note that $\boldsymbol{u}^{n+1}$ fulfills conditions (21) and also (22) thanks to equation (6). In order to compute $\boldsymbol{u}_i^{n+1}$ given a triangle T_i and the three values $(\boldsymbol{u}_i^{n+1} \cdot \boldsymbol{n})_\sigma$, $\forall \sigma \in E_i$, we solve the following set of three equations for the two variables a_i and b_i:

$$\begin{cases} \boldsymbol{u}_i^{n+1} = \begin{pmatrix} a_i \\ b_i \end{pmatrix} \\ \forall \sigma \in E_i, \quad \boldsymbol{u}_i^{n+1} \cdot \boldsymbol{n}_\sigma = \left(\boldsymbol{u}_i^{n+1} \cdot \boldsymbol{n}\right)_\sigma \end{cases}$$

This problem is, however, well posed, since we have also the following linear combination, based upon a geometrical property of triangles:

$$\begin{aligned} 0 = \boldsymbol{u}_i^{n+1} \cdot \sum_{\sigma \in E_i} l_\sigma \boldsymbol{n}_\sigma &= \sum_{\sigma \in E_i} l_\sigma \boldsymbol{u}_i^{n+1} \cdot \boldsymbol{n}_\sigma \\ &= \sum_{\sigma \in E_i} l_\sigma \left(\boldsymbol{u}_i^{n+1} \cdot \boldsymbol{n}\right)_\sigma \end{aligned}$$

4.2. Solving the complete set of equations

4.2.1. Source term for the convection and diffusion of the velocity

The source term for the convection and diffusion of the velocity is

$$\boldsymbol{s}^n = \boldsymbol{f}^n - \nabla p^n$$

Given a triangle T_i of the mesh, an integration of this expression on T_i yields

$$\int_{T_i} \boldsymbol{s}^n \, \mathrm{d}S = \int_{T_i} \boldsymbol{f}^n \, \mathrm{d}S - \oint_{\partial T_i} p^n \boldsymbol{n} \, \mathrm{d}\Gamma$$

A discrete form of the source term can eventually be obtained by computing approximations of p^n at the middle of the edges (see remark in Section 4.2.2). This is performed with the method exposed in Appendix A. Denoting p_σ^n the value computed that way, the discrete form of the source term is

$$S_i \boldsymbol{s}_i = S_i \boldsymbol{f} - \sum_{\sigma \in E_i} l_\sigma p_\sigma^n \boldsymbol{n} \tag{26}$$

4.2.2. Discretization of the source terms in the general case

A differentiation should be done between the source terms of the convection–diffusion equations, of the velocity components on the one hand, and of the passive scalar on the second hand.

In the second case indeed, if a physical property imposes a maximum principle for the concerned variable in the continuous equation itself, particular attention should be paid to preserve it in the discrete form. As shown in Appendix B, this can always be performed on meshes of the categories M_1 and M_2, by using a good discretization of the source terms (with the obvious preliminary condition that the maximum principle is preserved in the continuous system).

4.2.3. The complete algorithm

- Given an initial solution $\boldsymbol{u}_\mathrm{h}^{-1}$ which satisfies (21) and (22), and C_h^0,

- assuming $p_\mathrm{h}^{-1} = 0$,
- apply the projection operator:

$$\left(p_\mathrm{h}^0, \boldsymbol{u}_\mathrm{h}^0\right) = P\left(p_\mathrm{h}^{-1}, \boldsymbol{u}_\mathrm{h}^{-1}\right)$$

- Given $(\boldsymbol{u}_\mathrm{h}^n, p_\mathrm{h}^n)$, we obtain $(\boldsymbol{u}_\mathrm{h}^{n+1}, p_h^{n+1})$ by
  - prediction of the velocity field $\boldsymbol{u}_\mathrm{h}^*$:
    - compute the source term of CD_s thanks to equation (26),
    - apply the convection and diffusion operator: $\boldsymbol{u}_\mathrm{h}^* = CD_s(\boldsymbol{u}_\mathrm{h}^n)$,
  - apply the extension operator: $\boldsymbol{u}_\mathrm{h}^{**} = E(\boldsymbol{u}_\mathrm{h}^*)$,
  - apply the projection operator: $(p_\mathrm{h}^{n+1}, \boldsymbol{u}_\mathrm{h}^{n+1}) = P(p_\mathrm{h}^n, \boldsymbol{u}_\mathrm{h}^{**})$.
- Given C_h^n, apply the convection and diffusion operator: $C_\mathrm{h}^{n+1} = CD_0(u_\mathrm{h}^{n+1})$, where CD_0 denotes the convection and diffusion operator with a null source term.

5. NUMERICAL EXPERIMENTS

5.1. Numerical rate of convergence of the diffusion scheme

Our main goal was to verify the theoretical results presented in Section 3.2.3, and to analyze the convergence on meshes of the categories M_2 and M_3. This study was first presented in the unpublished report [11], and following is a short summary of the results.

5.1.1. Numerical results

On meshes of the category M_1, the measured rate of convergence for the tested regular solutions (see the expressions of u_1, u_2, u_3 and u_4 in *table I*) is 2. For an irregular solution (such as u_5 with a Dirac source point inside the domain), the measured rate of convergence is 1.

Note that u_5 is a Green function centered inside the domain. This solution is not regular enough for the proof of the error estimate (19) proposed in [2]. However, u_4, which has the same form, is regular enough since its source point is located outside the computational domain.

No violation of the maximum principle has been observed, which matches with the third property stated in Section 3.2.3.

Tests have been performed on both types of boundary conditions (Dirichlet or Neumann boundary conditions) showing that the type of boundary condition has no influence on the results.

TABLE I
Expression of the solutions tested in the numerical predictions of the diffusion problem of Section 3.2.

$u_1(x, y) = xy + y$	$\Delta u_1 = 0$
$u_2(x, y) = x^2 + y^2$	$\Delta u_2 = 4$
$u_3(x, y) = \sin(x + y)$	$\Delta u_3 = -2\sin(x + y)$
$u_4(x, y) = \frac{1}{2}\ln((x-1)^2 + (y-1)^2)$	$\Delta u_4 = \delta_{(1,1)}$
$u_5(x, y) = \frac{1}{2}\ln((x-1/7)^2 + (y-10/7)^2)$	$\Delta u_5 = \delta_{(1/7,10/7)}$

The measured rates of convergence obtained with meshes of the categories M_2 and M_3 are the same as with meshes of the category M_1. Moreover, the maximum principle is still fulfilled with meshes of the category M_2, which is in agreement with the theoretical results recalled in Section 3.2.3. Even more, the most amazing point is that using proposed extrapolation in the case of the category M_3 enables preserving this maximum principle.

A problem of definition of the transmittivity may appear as soon as two adjacent triangles have the same IOB. However, using a low threshold for the distance between two IOB (to avoid divisions by zero) solves this problem, as our computations performed on meshes with rectangles cut into two triangles show.

5.1.2. Conclusions

The results of numerical experiments are much better than the theoretical results obtained in [2]. There is, however, no contradiction; it simply means that, according to numerical results, the error estimate (19) obtained in [2] is probably not optimal.

Another interesting point is that the computed approximation is closer to the value of the exact solution at the IOB than at the center of gravity of the triangles, as we can see in *figure 4*, where two curves have been plotted.

- The first one is the convergence curve defined by the following quantity as a function of the mesh size h:

$$\log\left(\sqrt{\sum_{i=1}^{n} S_i\left(u_i - u(x_i)\right)^2}\right) \tag{27}$$

- The second one provides a comparison between the approximation computed in each triangle T_i and the value of the exact solution at the centroid x_i^G of T_i:

$$\log\left(\sqrt{\sum_{i=1}^{n} S_i\left(u_i - u\left(x_i^\mathrm{G}\right)\right)^2}\right) \tag{28}$$

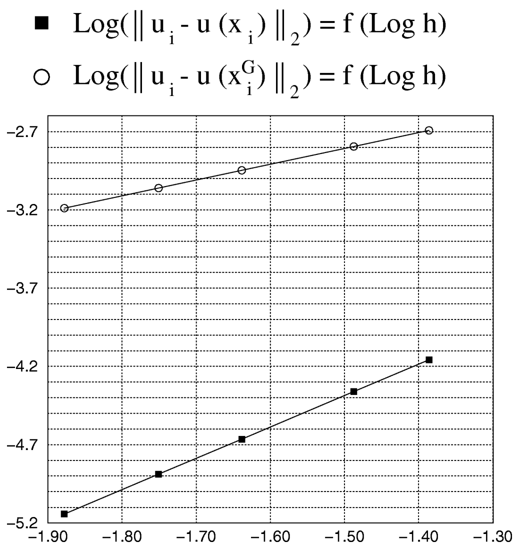

Figure 4. Convergence of $u_3(x, y) = \sin(x + y)$ on meshes of type M_3.

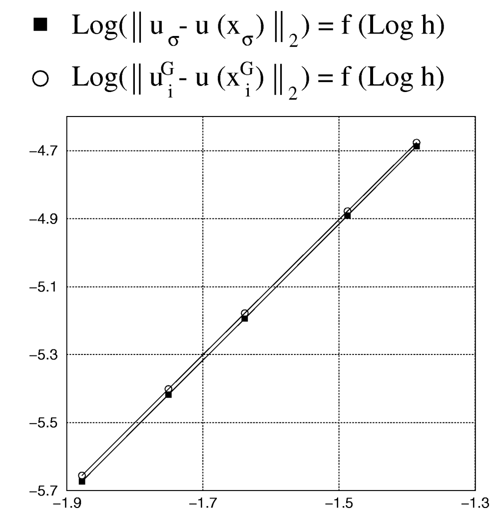

Figure 5. Convergence of $u_1(x, y) = xy + y$ on meshes of type M_3.

In the case of meshes of the category M_3, the maximum principle is apparently not fulfilled anymore if we associate the value of each IOB with its triangle itself, which is not adapted to the case where the IOB is outside the latter. However, using the method presented in Appendix A, an approximation of the variable at the center of gravity of each triangle can be computed. With these values, no violation of the discrete maximum principle could be detected in our tests. As can be seen in *figure 5*, the different interpolated values in these tests (not only the values at the center of gravity, but also at the middle

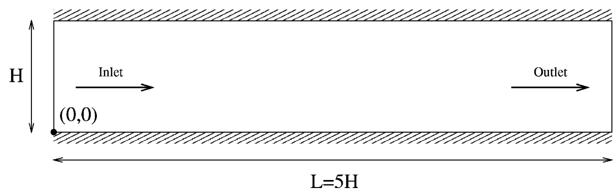

Figure 6. Geometrical description of the channel for Poiseuille flows computations.

of the edges) are also second-order accurate in respect to the mesh size h for regular solutions (and first-order accurate for irregular solution, such as u_5). In this figure, the following errors were plotted as functions of the mesh size h:

$$\log\left(\sqrt{\frac{\sum_{\sigma\in E} l_\sigma (u_\sigma - u(x_\sigma))^2}{\sum_{\sigma\in E} l_\sigma}}\right) \tag{29}$$

$$\log\left(\sqrt{\sum_{i=1}^{n} S_i \left(u_i^{\mathrm{G}} - u\left(x_i^{\mathrm{G}}\right)\right)^2}\right) \tag{30}$$

with

- E being the set of all the edges of the mesh,
- x_σ being the middle of the edge σ,
- u_σ being the value at the middle of the edge σ, computed as in Appendix A.2.2,
- u_i^{G} being the value at the center of gravity of the triangle T_i, computed as in Appendix A.2.4.

Note that the error (30) is different from both (27) and (28).

5.2. Poiseuille flow

5.2.1. Description of the numerical experiment

We study here the two-dimensional flow of an incompressible viscous fluid in a channel (see *figure 6*). The length and height of the channel are $L = 1$ and $H = 0.2$, respectively.

The necessary boundary conditions are:

- inlet: parabolic velocity profile

$$u_x(0, y) = \frac{y(H - y)}{(H/2)^2} U_{\max} \quad \text{and} \quad u_y(0, y) = 0$$

- outlet: uniform value for the pressure $p_{\mathrm{Outlet}} = 0$,
- walls: null velocity $\boldsymbol{u}_{\mathrm{Wall}} = \mathbf{0}$.

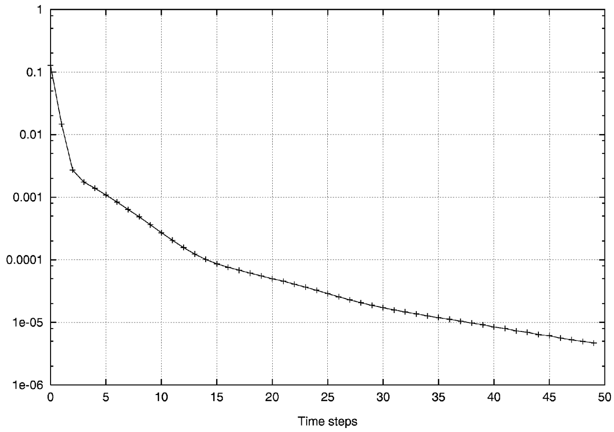

Figure 7. Convergence of the computation for $Re = 100$: $\|u_h^{n+1} - u_h^n\|_{L^2}$ as a function of the number of time steps (semi-structured mesh of 2 400 triangles).

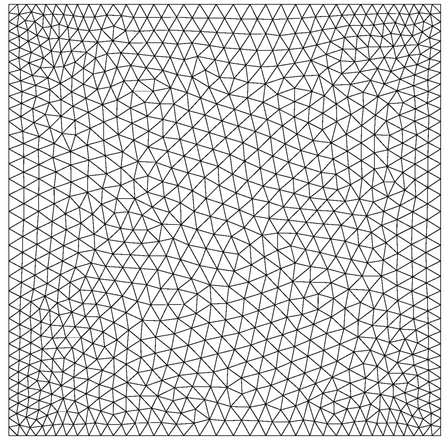

Figure 8. Unstructured mesh for computations of lid-driven cavity flows (1 872 elements).

The analytic solution of this problem is known all over the computational domain:

$$u_x(x, y) = \frac{y(H-y)}{(H/2)^2} U_{\max}$$
$$u_y(x, y) = 0$$
$$p(x, y) = -\frac{8\nu}{H^2} U_{\max}(x - L)$$

with ν being the kinematic viscosity of the fluid.

The Reynolds number is defined by

$$Re = \frac{U_{\max} L}{\nu}$$

with $U_{\max}$ being the maximum velocity. The computations were performed with Reynolds number 100.

5.2.2. Results

Many computations were performed with meshes of different types, from 600 to 11 045 triangles.

In every case, the convergence of the computation is good, as shown in *figure 7*. Most of the computations were performed on completely unstructured meshes, which are obviously not adapted to the flow structure. Poiseuille flows are so critical tests for the global scheme.

Even with semi-structured meshes (that is, obtained by dividing rectangles into two triangles), the convergence is fast and the results accurate, although the diffusion scheme is theoretically undefined in this case.

5.3. Lid-driven cavity flow

5.3.1. Description of the numerical experiment

The geometry of this problem is a squared cavity of size $L = 1$. The boundaries of the cavity are walls, except the upper boundary for which a uniform tangential velocity is prescribed ($u_x = 1$ and $u_y = 0$). Numerical results of this problem can be found in [13] and [14]. Two computations were performed in the present study, for Reynolds numbers of 400 and 1 000, respectively.

5.3.2. Results

In this case, an unstructured mesh of 1 872 elements has been used (see *figure 8*).

Both computations were performed with the same time step number $\tau = 1$. A converged solution is obtained after 100 time steps (see *figure 9*).

Figures 10 and *11* show streamlines and isobars for $Re = 400$ and 1 000, respectively. The results are in good agreement with the solutions presented in [14], in which the authors also use first order spatial approximation schemes.

The local characteristics are in good agreement with [14] as well, as can be seen on *figures 12* and *13*, where the velocity profiles along the vertical and horizontal centerlines of the cavity are represented.

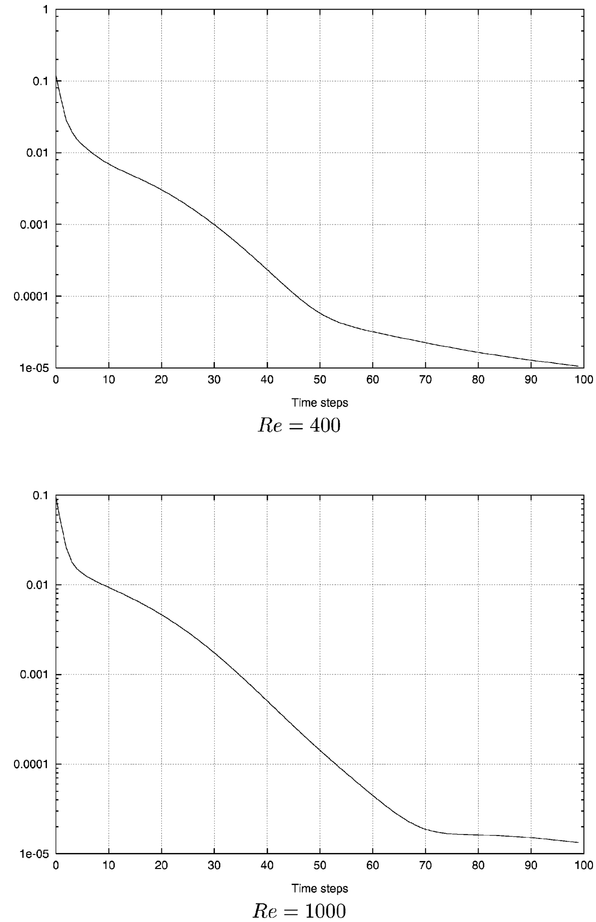

Figure 9. Convergence of the computations: $\|u_{\mathrm{h}}^{n+1} - u_{\mathrm{h}}^{n}\|_{L^2}$ as a function of the number of time steps performed.

5.4. Backward-facing step

5.4.1. Description of the numerical experiment

We consider here an incompressible two-dimensional viscous flow in a channel with a backward-facing step, as shown in *figure 14*.

Denoting h the dimension of the inlet of the channel, and H the height of the step, the value of the ratio H/h is 0.94.

The boundary conditions used in the computations are:

- inlet: parabolic velocity profile

$$u_x(0, y) = \frac{(y - H)(H + h - y)}{(h/2)^2} U_{\max} \quad \text{and}$$
$$u_y(0, y) = 0$$

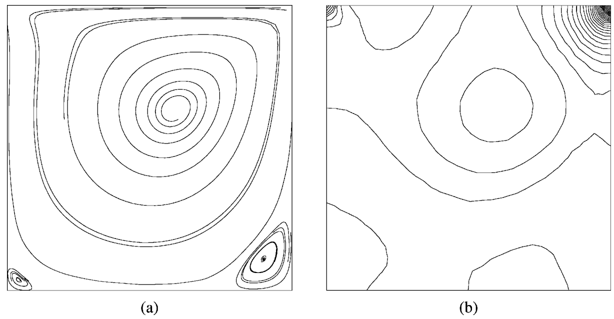

Figure 10. Streamlines (a) and isobars (b) for $Re = 400$.

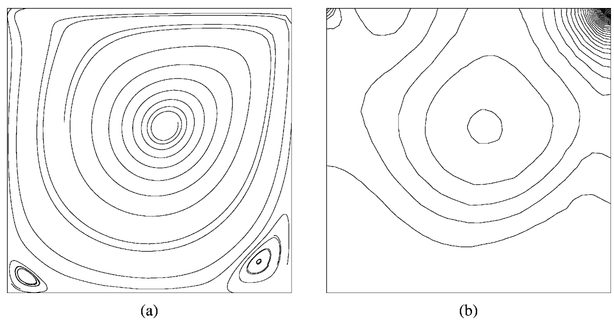

Figure 11. Streamlines (a) and isobars (b) for $Re = 1\,000$.

- outlet: uniform value for the pressure $p_{\text{Outlet}} = 0$,
- walls: null velocity $\boldsymbol{u}_{\text{Wall}} = \mathbf{0}$.

The Reynolds number is defined by

$$Re = \frac{\frac{2}{3} U_{\max} 2h}{\nu}$$

The computations were performed for the following Reynolds numbers, for comparison with the results obtained in [15] (an experimental study), [9, 16] (numerical studies): 50, 100, 200, 300, 400, 500, 600.

5.4.2. Results

The mesh we used for all the following computations is a semi-structured grid of 1 720 triangles. The solutions have rapidly converged with high time step numbers, thanks to the implicit scheme (see *figure 15*).

The lower reattachment length is plotted as a function of the Reynolds number in *figure 16*. A comparison with the results of [9, 15, 16] shows that the reattachment length is slightly underestimated. For high values of the Reynolds number, a secondary recirculation region appears near the upper wall of the channel, downstream from the previous one. In the present study, this recirculation region appears only for a Reynolds number of 600.

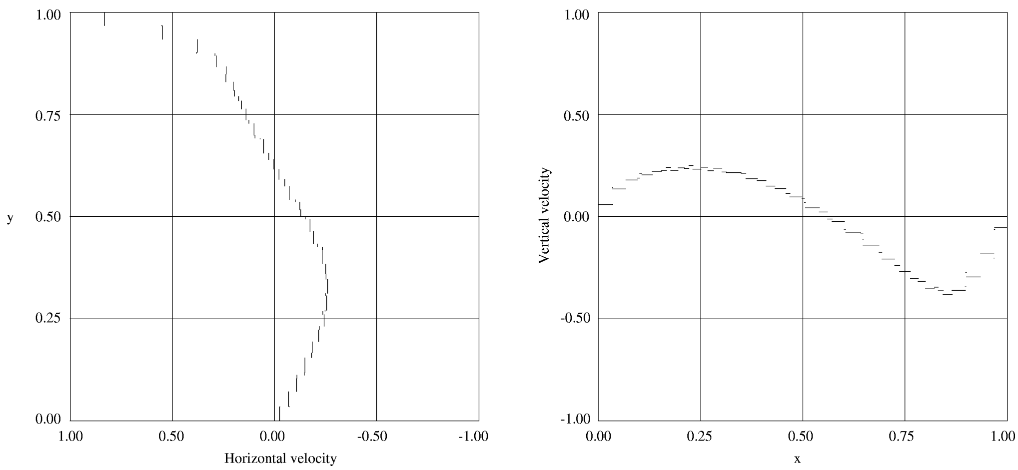

Figure 12. Velocity profiles along the centerlines of the cavity for $Re = 400$.

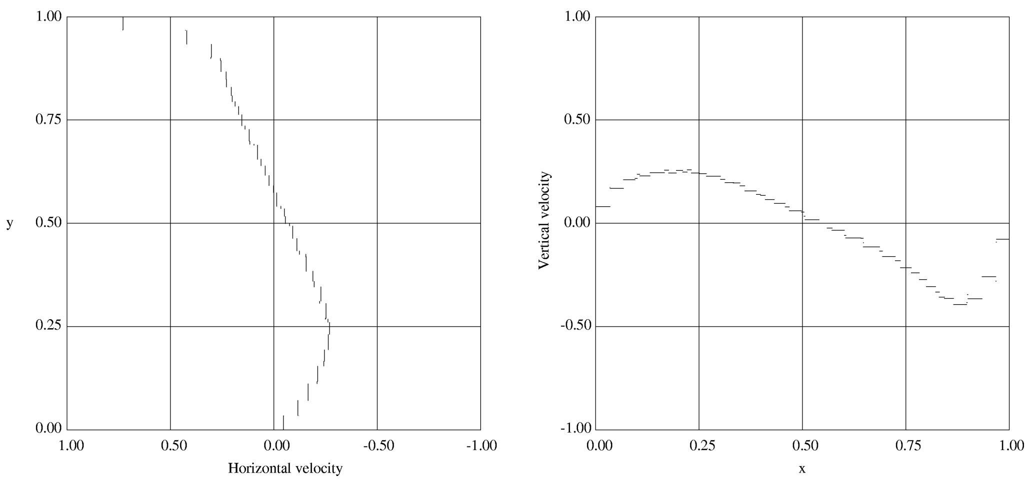

Figure 13. Velocity profiles along the centerlines of the cavity for $Re = 1\,000$.

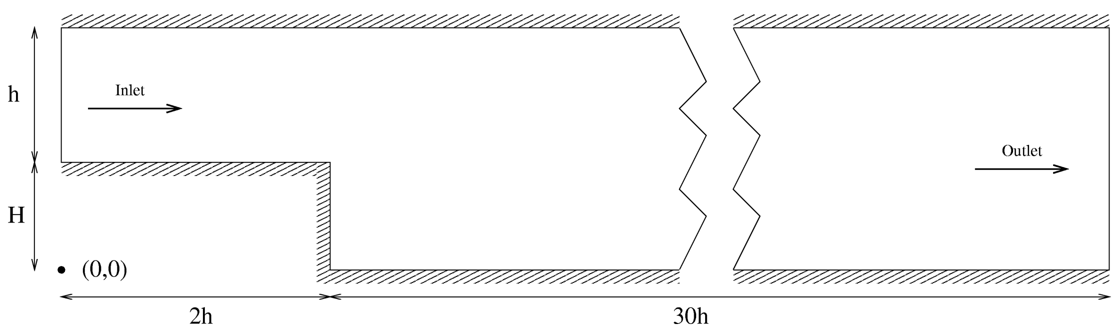

Figure 14. Geometrical description of the backward-facing step.

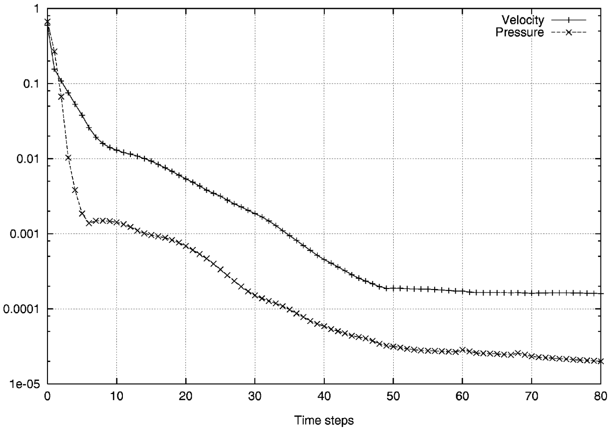

Figure 15. Convergence of the computation for $Re = 300$ and $\tau = 20$: $\|w_h^{n+1} - w_h^n\|_{L^2}$ as a function of the number of time steps, for both the velocity and the pressure.

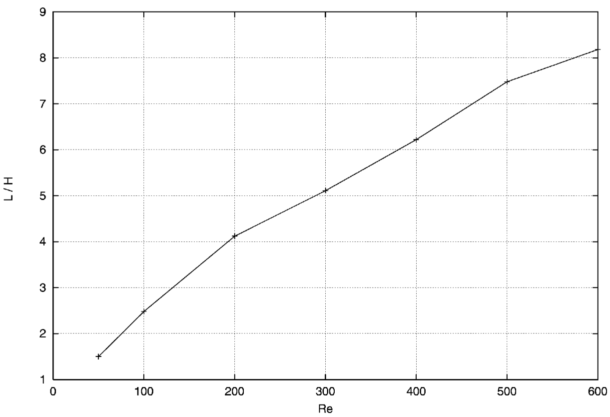

Figure 16. Lower reattachment length L/H as a function of the Reynolds number Re.

Obviously, the grid is too coarse for this problem. However, these results show the ability of the method to predict such channel flows.

5.5. Natural convection in a square cavity

5.5.1. Problem and equations

The problem being considered here was extensively studied in [17, 18]. It is the problem of a two-dimensional flow of a Boussinesq fluid of Prandtl number 0.71 in an upright square cavity of side L. Both velocity components are zero on the boundaries. The horizontal walls are insulated, and the left and right vertical sides are at temperatures T_h and T_c, respectively.

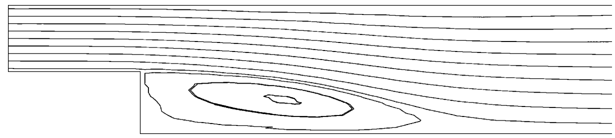

Figure 17. Streamlines for $Re = 300$.

The quantities L, L^2/κ (with κ being the constant thermal diffusivity) and $\rho\kappa^2/L^2$ are used as scale factors for length, time and pressure, respectively. We denote $\theta = (T - T_c)/\Delta T$ with $\Delta T = T_h - T_c$ and T being the local dimensional temperature of the fluid. The nondimensional equations are then

$$\begin{aligned} &\nabla^* \cdot \boldsymbol{v}^* = 0 \\ &\frac{\partial \boldsymbol{v}^*}{\partial t^*} + \left(\boldsymbol{v}^* \cdot \nabla^*\right)\boldsymbol{v}^* + \nabla^* p^* - Pr\,\Delta^* \boldsymbol{v}^* = Ra\,Pr\,\theta \boldsymbol{k} \\ &\frac{\partial \theta}{\partial t^*} + \left(\boldsymbol{v}^* \cdot \nabla^*\right)\theta - \Delta^* \theta = 0 \end{aligned} \qquad (31)$$

with

- $Ra = \beta g \Delta T L^3/(\kappa\nu)$ being the Rayleigh number, β being the coefficient of volumetric expansion, g being the gravity and ν being the kinematic viscosity;
- $Pr = \nu/\kappa$ being the Prandtl number ($Pr = 0.71$ in our case);
- $\boldsymbol{k}$ being the vertical descending unit vector.

As we can see, the set of equations (31) is formally identical to (1), (2), (3).

The source term $\boldsymbol{s} = Ra\,Pr\,\theta\boldsymbol{k}$ of the second equation is approximated, for a given triangle T_i at the date t^{n+1}, by

$$\boldsymbol{s}_i^{n+1} = S_i Ra\,Pr\,\theta_i^n \boldsymbol{k}$$

with S_i being the surface of T_i.

The computations were performed with Rayleigh numbers of 10^3 and 10^6 on uniform unstructured meshes of 1 872 elements and 11 434 elements, respectively.

5.5.2. Results

Following are results compared with the bench mark solutions obtained in [18]. For a qualitative comparison, contour plots of the velocity components, the pressure and the temperature are given (see *figures 18–21*).

Moreover, some characteristic numerical values are supplied for a quantitative comparison (see *tables II* and *III*):

- the maximum vertical velocity on the horizontal mid-plane ($u_{\max}^{x=1/2}$) and its location ($y_{\max}$),

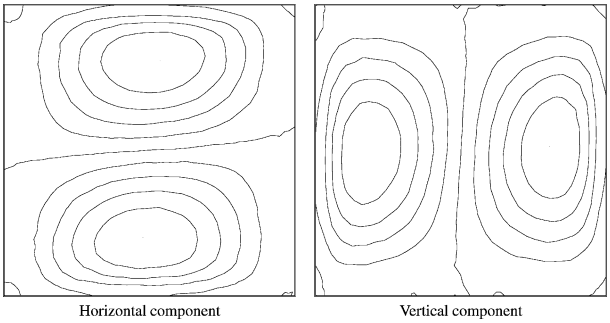

Figure 18. Contours of the velocity components of our solution at $Ra = 10^3$. (a) Contours at -3.558 (0.7125) 3.567. (b) Contours at -3.612 (0.7211) 3.599.

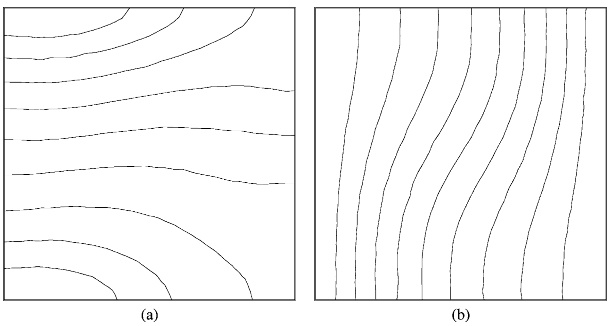

Figure 19. Contours of the pressure (a) and temperature (b) of the solution at $Ra = 10^3$. (a) Contours at -67 (45.8) 391. (b) Contours at 0 (0.1) 1.

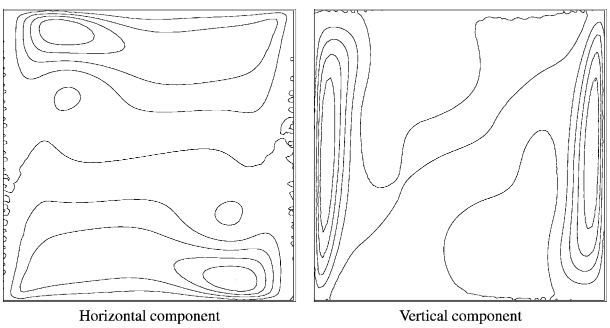

Figure 20. Contours of the velocity components of our solution at $Ra = 10^6$. (a) Contours at -125.74 (25.08) 125.07. (b) Contours at -215.27 (43.19) 216.61.

- the maximum horizontal velocity on the vertical mid-plane ($v_{\max}^{y=1/2}$) and its location ($x_{\max}$),
- the average Nusselt number on the vertical mid-plane

$$Nu_{1/2} = \int_0^1 \left(u(y)T(y) - \left.\frac{\partial T}{\partial x}\right|_{x=1/2}(y) \right) \mathrm{d}y$$

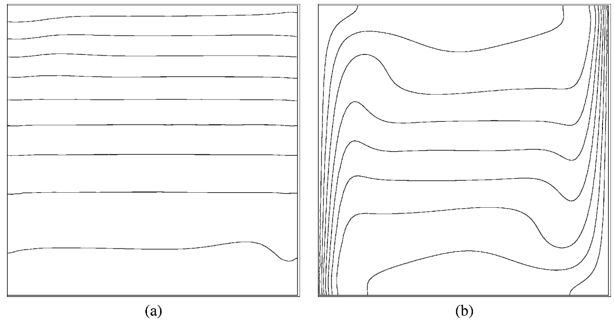

Figure 21. Contours of the pressure (a) and temperature (b) of the solution at $Ra = 10^6$. (a) Contours at $-18\,742$ (39 032.6) 371 584. (b) Contours at 0 (0.1) 1.

TABLE II
Comparison between our solution and the bench mark solution at $Ra = 10^3$.

	$u_{\max}^{x=1/2}$ ($y_{\max}$)	$v_{\max}^{y=1/2}$ ($x_{\max}$)	$Nu_{1/2}$
Bench mark solution	3.649 (0.813)	3.697 (0.178)	1.118
Our solution	3.603 (0.814)	3.646 (0.174)	1.106

TABLE III
Comparison between our solution and the bench mark solution at $Ra = 10^6$.

	$u_{\max}^{x=1/2}$ ($y_{\max}$)	$v_{\max}^{y=1/2}$ ($x_{\max}$)	$Nu_{1/2}$
Bench mark solution	64.63 (0.850)	219.36 (0.0379)	8.799
Our solution	67.96 (0.854)	219.20 (0.0405)	9.467

These results are in good agreement with the bench mark solutions. Note that the lack of accuracy of the convection scheme used for these computations may be responsible for small differences (especially in the case where $Ra = 10^6$). This could easily be improved using a method such as MUSCL.

6. CONCLUSION

A solver for the Navier–Stokes equations has been proposed to simulate incompressible viscous flows and a convection and diffusion problem for a passive scalar quantity. This solver is based upon a fractional time step scheme and the finite volume method on unstructured triangular meshes. We emphasize that the accuracy of the diffusion scheme is of prime importance to get a reliable pressure–velocity correction step, and also, of course, to compute diffusive terms in scalar equations and in momentum governing equation. Up to the authors, measured second-order accuracy of the diffusion scheme based on the IOB, which differs from the theoretical one which is proved to be one, is worth being known. It nevertheless requires that one works with both cell averaged values and approximations at the IOB.

The numerical method is simple and is a good compromise between computation time and accuracy, especially due to the diffusion scheme. The convection scheme's accuracy may be improved using currently proposed interpolation and a reconstruction method such as MUSCL.

The three-dimensional extension of the method is feasible using tetrahedra. Moreover, an extension to flows of variable viscosity fluids and to turbulent models such as k–ε can be performed. However, this requires providing an accurate approximation of the gradient of a scalar variable on each interface, and not only the normal derivative. Indeed, in the general case $\nabla \cdot (\mu_{\text{eff}}(\nabla \boldsymbol{u} + \nabla^{\text{t}}\boldsymbol{u})) \neq \nabla \cdot (\mu_{\text{eff}}\nabla \boldsymbol{u})$, although the equality is true in the present paper since $\nabla \boldsymbol{u} = 0$ and $\mu_{\text{eff}} = \mu_0$ is constant. A first proposition for such an approximation is provided and analyzed in [11]. However, it is not clear whether this one is good enough, and it anyway requires much more numerical and theoretical investigation. We thus believe that the implementation of turbulent models is far beyond the purpose of the present work, since no theoretical proof of convergence is available in this area by now.

Acknowledgements

Part of this work has benefited from fruitful discussions with Prof. Thierry Gallouët. Financial support has been provided by Électricité de France under EDF contract AEE256/B02501. Computational facilities were provided by Université Laval, Québec.

REFERENCES

[1] Gallouët T., An introduction to finite volume methods, in: Problèmes non linéaires appliqués : Méthodes de volumes finis, Écoles CEA-EDF-INRIA, 1992.

[2] Eymard R., Gallouët T., Herbin R., Finite volume methods, in: Ciarlet P.G., Lions J.L. (Eds.), Handbook of Numerical Analysis, North-Holland, to appear.

[3] Champier S., Gallouët T., Convergence d'un schéma décentré amont sur un maillage triangulaire pour un problème hyperbolique linéaire, Math. Mod. Numer. Anal. 26 (1992) 835–853.

[4] Faille I., Modélisation bidimensionnelle de la genèse et de la migration des hydrocarbures dans un bassin sédimentaire, Thèse de doctorat de l'Université Joseph Fourier, Grenoble I, 1992.

[5] Faille I., A control volume method to solve an elliptic equation on a two-dimensional irregular mesh, Comput. Methods Appl. Mech. Engrg. 100 (1992) 275–290.

[6] Baranger J., Maître J.F., Oudin F., Application de la théorie des éléments finis mixtes à l'étude d'une classe de schémas aux volumes différences finis pour les problèmes elliptiques, C.R. Acad. Sci. Paris Série I 319 (1994) 401–404.

[7] Baranger J., Maître J.F., Oudin F., Connection between finite volume and mixed finite element methods, Math. Mod. Numer. Anal. 30 (4) (1996) 445–465.

[8] Cai Z., Mandel J., McCormick S., The finite volume element method for diffusion equations on general triangulations, SIAM J. Numer. Anal. 28 (2) (1991) 392–402.

[9] Boivin S., Hérard J.M., Résolution des équations de Navier–Stokes par la méthode des volumes finis sur maillage non structuré, Rapport EDF HE-41/96/004/B, 1996.

[10] Chorin A.J., Numerical solution of the Navier–Stokes equations, Math. Comput. 22 (1968).

[11] Cayré F., Schémas volumes finis pour un problème elliptique sur maillage triangulaire — Etude numérique de convergence, Rapport EDF HE-41/97/057/A, 1997.

[12] Herbin R., An error estimate for a finite volume scheme for a diffusion–convection problem on a triangular mesh, Numer. Methods Part. Diff. Eq. 11 (1995) 165–173.

[13] Ghia U., Ghia K.N., Shin C.T., High-*Re* solutions for incompressible flow using the Navier–Stokes equations and a multigrid method, J. Comput. Phys. 48 (1982) 387–411.

[14] Churbanov A.G., Pavlov A.N., Vabishchevich P.N., Operator-splitting methods for the incompressible Navier–Stokes equations on non-staggered grids, Int. J. Numer. Methods Fluids 21 (1995) 617–640.

[15] Armaly B.F., Durst F., Pereira J.C.F., Schönung B., Experimental and theoretical investigation of backward-facing step flow, J. Fluid Mech. 127 (1983) 473–496.

[16] Barton I.E., A numerical study of flow over a confined backward-facing step, Int. J. Numer. Methods Fluids 21 (1995) 653–665.

[17] De Vahl Davis G., Jones I.P., Natural convection in a square cavity: a comparison exercise, Int. J. Numer. Methods Fluids 3 (1983) 227–248.

[18] De Vahl Davis G., Natural convection of air in a square cavity: a bench mark solution, Int. J. Numer. Methods Fluids 3 (1983) 249–264.

APPENDIX A

Local interpolation method on triangular meshes

A.1. Problem

The upwind convection scheme presented previously (see Section 3.1) requires that a value of the convected variable *inside the cell* is provided, in order to compute a correct flux through the edges. Otherwise, the upwinding becomes a "downwinding" for each edge with negative transmittivity, which might result in a local lack of stability of the convection scheme.

Moreover, in order to compute good approximations of integrals on a cell, such as

$$\int_{T_i} \frac{\partial w_\mathrm{h}}{\partial t}\,\mathrm{d}\Omega$$

values of the discrete variable w_h inside the triangles are necessary.

A.2. Method

The method described below is based on the following observation. Let u_i be the approximation obtained for the triangle T_i with the diffusion scheme presented above. Let x_i and x_i^G be the IOB and the centroid of T_i, respectively. As will be seen in Section 5.1, u_i is a second-order approximation of $u(x_i)$ and, consequently, a first-order approximation of $u(x_i^\mathrm{G})$. This leads to use u_i as a good enough representation of the exact solution at the IOB, in order to get a new approximation of u at the centroid, denoted later on $G_i(u_\mathrm{h})$. In order to compute this value, we first need to compute approximations of u at the middle of all the edges of the mesh.

A.2.1. Interpolation at the middle of the internal edges

Let be given an internal edge σ_{ij}, common to the triangles T_i and T_j whose IOB are x_i and x_j, respectively (see *figure 3*). Denoting x_{ij} as the middle of σ_{ij}, the three points x_i, x_j and x_{ij} are aligned. Therefore, x_{ij} can be considered as the center of gravity of the system:

$$\left\{(x_i, t_{ij}); (x_j, 1-t_{ij})\right\}, \quad \text{where}$$
$$t_{ij} = \frac{(x_j - x_{ij})(x_j - x_i)}{(x_j - x_i)^2}$$

Assume that the computation leads to first- or second-order approximations of the exact solution at the IOB of T_i and T_j, denoted u_i and u_j, respectively. Then this level of accuracy is preserved for the middle of the edge σ_{ij}, with the following choice:

$$u_{ij} = t_{ij}u_i + (1-t_{ij})u_j \tag{A.1}$$

A.2.2. Interpolation at the middle of the boundary edges

Let σ be a boundary edge included in the triangle T_i. If a Dirichlet condition applies to σ, no approximation is needed for the value of the exact solution at the middle of σ, since this value is given. If a Neumann condition applies, the given value is the exact flux F_σ, and the natural choice for the approximation at the middle of σ is u_σ such that

$$F_\sigma = \tau_\sigma(u_i - u_\sigma), \quad \text{i.e.} \quad u_\sigma = u_i - \frac{F_\sigma}{\tau_\sigma}$$

If u_i is a second-order approximation of the exact solution at the IOB of T_i, then u_σ is also a second-order approximation of the exact solution at the middle of σ.

A.2.3. Case of a boundary edge without any boundary condition

Let σ be a boundary edge where no boundary condition applies, x_σ its middle, T_i the triangle including σ. Even in this case, a good approximation u_σ of the solution at x_σ can generally be computed.

However, if T_i has only one adjacent triangle (i.e. it has two edges on the boundary), the approximation we choose is simply $u_\sigma = u_i$, which is a first-order approximation.

In the opposite case, the values u_j and u_k of the two triangles T_j and T_k adjacent with T_i can be used to compute a more accurate approximation:

$$u_\sigma = u_i + \frac{\tau_{\sigma_{ij}}(u_i - u_j) + \tau_{\sigma_{ik}}(u_i - u_k)}{\tau_\sigma}$$

Note that if u_i, u_j and u_k are second-order approximations of the exact solution at the IOB of T_i, T_j and T_k, respectively, then u_σ is a second-order approximation of the exact solution at the middle of σ.

A.2.4. Interpolation at every point of the domain

Let M be a point of a triangle T_i of the mesh. Let x_{σ_1}, x_{σ_2}, x_{σ_3} be the middles of the edges σ_1, σ_2, σ_3 of T_i, and let u_{σ_1}, u_{σ_2}, u_{σ_3} be second-order approximations of the exact solution at these points. Denoting α and β two real numbers such that M is the center of gravity of the system [2]

$$\left\{(x_{\sigma_1}, \alpha); (x_{\sigma_2}, \beta); (x_{\sigma_3}, 1-\alpha-\beta)\right\}$$

[2] That is, such that $\alpha(x_M - x_{\sigma_1}) + \beta(x_M - x_{\sigma_2}) + (1-\alpha-\beta)(x_M - x_{\sigma_3}) = \mathbf{0}$.

a second-order approximation of the exact solution at the point M is

$$u_M = \alpha u_{\sigma_1} + \beta u_{\sigma_2} + (1-\alpha-\beta) u_{\sigma_3}$$

An important case for M is when it is the centroid G_i of T_i (i.e. $\alpha = \beta = 1/3$):

$$u_i^{\mathrm{G}} = \frac{u_{\sigma_1} + u_{\sigma_2} + u_{\sigma_3}}{3} \tag{A.2}$$

The combination of the equations (A.1) and (A.2) give us a discrete operator G of second-order accuracy locally. From a field defined at the IOB, the application of this operator yields a field defined at the centroid of the triangles of the mesh. The value of this last field for a discrete variable w_{h}, at the centroid of the triangle T_i ($i \in \{1, 2, \ldots, N\}$), is denoted $G_i(w_{\mathrm{h}})$.

APPENDIX B

Convection–diffusion equation: source term discretization and preservation of the maximum principle

In this appendix, we examine how the source term should be discretized to preserve the maximum principle when solving a convection–diffusion equation on meshes of the categories M_1 and M_2.

B.1. Equation. Properties of the matrix of the system

B.1.1. Matrix form of the system

We discretize here the following equation, given some initial conditions for ϕ:

$$\frac{\partial \phi}{\partial t} + \nabla \cdot (\phi \boldsymbol{u}) - \nabla \cdot (\kappa \nabla \phi) = s \tag{B.1}$$

with ϕ being the scalar unknown, $\boldsymbol{u}$ being the divergence free velocity field, and s being the source term.

As a seek for simplicity of the matrix form that follows, we assume homogeneous Neumann boundary conditions for ϕ ($(\partial\phi/\partial\boldsymbol{n})|_\Gamma = 0$), and a tangent velocity field on the boundary ($\boldsymbol{u} \cdot \boldsymbol{n}|_\Gamma = 0$).

The matrix form of the scheme described in Sections 3.1 and 3.2 writes:

$$\underbrace{(D + A^{\mathrm{conv}} + A^{\mathrm{diff}})}_{B} \phi^{n+1} = D\phi^n + \delta t D s^n$$

with

- $\forall i \in \{1, 2, \ldots, N\}, \forall j \in \{1, 2, \ldots, N\},\ j \neq i,$

$$D_{ii} = \frac{\Omega_i}{\delta t}, \qquad D_{ij} = 0$$

- $\forall i \in \{1, 2, \ldots, N\}, \forall k \in V(i),$

$$\begin{cases} A_{ii}^{\mathrm{conv}} = \displaystyle\sum_{j \in v(i)} l_{ij} (\boldsymbol{u} \cdot \boldsymbol{n})_{ij} \alpha_{ij} \\ A_{ik}^{\mathrm{conv}} = l_{ik} (\boldsymbol{u} \cdot \boldsymbol{n})_{ik} (1 - \alpha_{ik}) \end{cases}$$

(other coefficients $= 0$);

- $\forall i \in \{1, 2, \ldots, N\}, \forall k \in V(i),$

$$\begin{cases} A_{ii}^{\mathrm{diff}} = \displaystyle\sum_{j \in v(i)} \tau_{ij} \\ A_{ik}^{\mathrm{diff}} = -\tau_{ik} \end{cases}$$

(other coefficients $= 0$);

- s^n being a discrete form of the continuous source term s, such that the discrete maximum principle is preserved.

B.1.2. Properties of the matrices

PROPOSITION. – *On meshes of the categories M_1 and M_2, D is a diagonal matrix and B is a matrix with strictly dominant diagonal, such that*

- $\forall i \in \{1, 2, \ldots, N\}$, $D_{ii} > 0$*;*
- $\forall i \in \{1, 2, \ldots, N\}$, $B_{ii} > 0$ *and* $\forall i \in \{1, 2, \ldots, N\}$, $\forall j \in \{1, 2, \ldots, N\}$, $j \neq i$, $B_{ij} \leq 0$.

Proof. –

- $\forall i \in \{1, 2, \ldots, N\}$, $D_{ii} = \Omega_i / \delta t > 0$.
- As
  - $\forall i \in \{1, 2, \ldots, N\}$, $\forall j \in \{1, 2, \ldots, N\}$, $j \neq i$, $A_{ii}^{\mathrm{conv}} \geq 0$ and $A_{ij}^{\mathrm{conv}} \leq 0$, according to the definition of α_{ij}, and
  - $\forall i \in \{1, 2, \ldots, N\}$, $\forall j \in \{1, 2, \ldots, N\}$, $j \neq i$, $A_{ii}^{\mathrm{diff}} \geq 0$ and $A_{ij}^{\mathrm{diff}} \leq 0$ because for meshes of the categories M_1 and M_2, $\tau_{ij} > 0$,

  then $\forall i \in \{1, 2, \ldots, N\}$, $\forall j \in \{1, 2, \ldots, N\}$, $j \neq i$,

$$B_{ii} = D_{ii} + A_{ii}^{\mathrm{conv}} + A_{ii}^{\mathrm{diff}} > 0 \quad \text{and}$$
$$B_{ij} = A_{ij}^{\mathrm{conv}} + A_{ij}^{\mathrm{diff}} \leq 0$$

- And finally, as
  - $\forall i \in \{1, 2, \ldots, N\}$,

$$\sum_{j\in\{1,2,\ldots,N\}} A_{ij}^{\mathrm{conv}} = \sum_{j\in v(i)} l_{ij}(\boldsymbol{u}\cdot\boldsymbol{n})_{ij} = 0$$

  ($\boldsymbol{u}$ is divergence-free),
  - $\forall i \in \{1, 2, \ldots, N\}$,

$$\sum_{j\in\{1,2,\ldots,N\}} A_{ij}^{\mathrm{diff}} = 0$$

then

$$\forall i \in \{1, 2, \ldots, N\}, \quad B_{ii} + \sum_{j\in\{1,2,\ldots,N\}-\{i\}} B_{ij} = D_{ii} > 0$$

As a consequence, the matrix B has an inverse B^{-1} which coefficients are positive numbers. In the following, this property will be denoted

$$B^{-1} \geq \boldsymbol{O} \tag{B.2}$$

B.2. Discrete form of the source term to preserve the principle of maximum

B.2.1. Definition of the discrete form of the source term

We suppose here that the variable ϕ of problem (B.1) is such that $0 \leq \phi \leq 1$. The continuous principle of maximum is supposed to be preserved (thanks to a convenient physical model), and so the source term is such that

- considering the following (possibly nonlinear) system with initial condition

$$\begin{cases} \dfrac{\mathrm{d}f^n}{\mathrm{d}t}(t) = s\big(f^n(t)\big) \\ f^n(n\Delta t) = \phi^n, \quad 0 \leq \phi^n \leq 1 \end{cases} \tag{B.3}$$

- this problem has a unique solution such that $0 \leq f^n((n+1)\Delta t) \leq 1$.

Given this property and the analytical solution $f^n(t)$ of the problem, we build the following time-consistent approximation of the source term:

$$s_{\mathrm{h}}^n = \frac{f^n((n+1)\Delta t) - f^n(n\Delta t)}{\Delta t}$$

B.2.2. Proof of the preservation of the discrete maximum principle

With the previous notations, the discrete system writes

$$\begin{aligned} B\phi^{n+1} &= D\phi^n + \Delta t D S_{\mathrm{h}}^n \\ &= Df^n\big((n+1)\Delta t\big) \end{aligned} \tag{B.4}$$

where

- $f^n = (f_1^n, f_2^n, \ldots, f_N^n)^{\mathrm{T}}$, f_i^n is the solution of problem (B.3) with the initial condition $f_i^n(n\Delta t) = \phi_i^n$;
- $S_{\mathrm{h}}^n = (s_{\mathrm{h},1}^n, s_{\mathrm{h},2}^n, \ldots, s_{\mathrm{h},N}^n)^{\mathrm{T}}$ with

$$s_{\mathrm{h},i}^n = \frac{f_i^n((n+1)\Delta t) - f_i^n(n\Delta t)}{\Delta t}$$

Denote $\psi = 1 - \phi$, and suppose $\forall i \in \{1, 2, \ldots, N\}$, $0 \leq \phi_i^n \leq 1$ (denoted $\mathbf{0} \leq \phi^n \leq \mathbf{1}$ in the following), then

- $\mathbf{0} \leq \phi^{n+1} = B^{-1}Df^n((n+1)\Delta t)$ as $B^{-1} \geq \boldsymbol{O}$, $D \geq \boldsymbol{O}$ and $f^n((n+1)\Delta t) \geq \mathbf{0}$;
- $\psi^n \geq \mathbf{0}$, and as $A^{\mathrm{conv}}\mathbf{1} = A^{\mathrm{diff}}\mathbf{1} = \mathbf{0}$:

$$\begin{aligned} B\psi^{n+1} &= B\mathbf{1} - B\phi^{n+1} \\ &= B\mathbf{1} - Df^n\big((n+1)\Delta t\big) \\ &= D\big(\mathbf{1} - f^n\big((n+1)\Delta t\big)\big) \end{aligned}$$

As a result, $\psi^{n+1} = \mathbf{1} - \phi^{n+1} \geq \mathbf{0}$.

This ends the demonstration by proving that

$$(\mathbf{0} \leq \phi^n \leq \mathbf{1}) \Rightarrow (\mathbf{0} \leq \phi^{n+1} \leq \mathbf{1})$$

B.3. Conclusion

With a correct discrete form of the source term (defined in Appendix B.2.1), the properties of the global scheme produced in Appendix B.1, for meshes of the categories M_1 and M_2, enable proving that the discrete maximum principle is preserved. This is a crucial characteristic of the scheme, which ensures that problems encountered in classical industrial applications, such as natural convection near a wall, will never lead to nonphysical values of the variables (under the assumption that the physical model is convenient, in the sense of Appendix B.2.1).

Concerning meshes of the category M_3, the extrapolation method presented in Appendix A should ensure that the maximum principle is also preserved: although we did not prove that theoretically, we could not exhibit any violation during our numerical tests.

B.4. Example

In the following example, we consider the problem

$$\frac{\partial \phi}{\partial t} + \nabla \cdot (\phi \boldsymbol{u}) - \nabla \cdot (\kappa \nabla \phi) = s = \lambda \phi (1 - \phi), \qquad \lambda \in \Re$$

The analytical resolution of problem (B.3) yields

$$s^n_{\mathrm{h},i} = \frac{f^n_i((n+1)\Delta t) - f^n_i(n\Delta t)}{\Delta t}$$
$$= \frac{\phi^n_i(1-\phi^n_i)(\mathrm{e}^{\lambda_i \Delta t} - 1}{\Delta t[\phi^n_i(\mathrm{e}^{\lambda_i \Delta t} - 1) + 1]}$$

Now we can check that

$$\left(0 \le \phi^n_i \le 1\right) \Rightarrow \left(0 \le f^n_i\left((n+1)\Delta t\right) \le 1\right)$$

- if $\phi^n_i = 1$ then $f^n_i((n+1)\Delta t) = 1$;
- if $0 \le \phi^n_i < 1$, let

$$G = \frac{\phi^n_i}{1-\phi^n_i}\mathrm{e}^{\lambda_i \Delta t}$$

Then

$$f^n_i\left((n+1)\Delta t\right) = \frac{G}{1+G}$$

and so

$$0 \le f^n_i\left((n+1)\Delta t\right) < 1$$